DOI: 10.17344/acsi.2025.9670 *Acta Chim. Slov.* **2026,** *73,* 496–513
creative commons

Scientific paper

Carbon dots loaded suppository containing D-mannose as a strategy against *E. coli* mediated vaginosis: An *in vitro* feasibility analysis

Debaprasad Routray,[1] Bhabani Sankar Satapathy,[2] Himansu Bhusan Samal,[1] Gurudutta Pattnaik[1]*

[1] *Centurion University of Technology & Management, Bhubaneswar, Odisha, India*

[2] *GITAM School of Pharmacy, GITAM Deemed to be University, Hyderabad Campus, Telangana, India*

* *Corresponding author: E-mail: guruduttapatnaik@gmail.com gurudutta.pattnaik@cutm.ac.in*

Received: 12-02-2025

Abstract

Effective treatment of bacterial vaginosis (BV) remains a staggering task till today. This study proposes a novel strategy using nitrogen-doped carbon dots (N@CDs) embedded in a Dmannose suppository. N@CDs were synthesized via a one-pot hydrothermal method, characterized using HR-TEM, particle size (5.2 nm), zeta potential (–16.23 mV), XRD, photoluminescence intensity and Raman spectroscopy. The suppository, optimized through central composite design, was evaluated for hardness, melting point (35–40 °C), disintegration, mucoadhesion (4.9 ± 0.20 dyne/cm^2×10^2), liquefaction (10.5 min), and reasonable antibacterial activity. FTIR confirmed no major excipient interactions. Further *in vivo* studies on BV induced animal model are underway for the future clinical viability of experimental N@CDs.

Keywords: N-doped Carbon Dots, Suppository, Optimization, Mucoadhesion

1. Introduction

Bacterial vaginosis (BV) has been a worrisome medical condition among women across the globe.[1] At present, 23–29% of women suffer from BV, among which *E. coli* mediated BV(accounting for nearly 28% of BV cases) are one of the most common type infections.[2] Effective treatment of BV remains a challenge owing to unique vaginal microenvironment, change in pH, enzymatic action, high mucus turnover etc.[3] If untreated/neglected, BV leads to severe form of systemic infections. Additionally, the chances of clinical recurrence and antibiotic resistance are major limitations associated with conventional treatment approaches.[4] Studies have indicated that upon discontinuing prophylaxis, infection incidence returns to pre-treatment levels within three months in the case of routine drug therapy. Thus, there has been an urgent need for a local, effective and painless treatment alternative to address BV.

In this context, carbon dots (CDs) have emerged as a potential therapeutic option to treat microbial infections.[5] Since carbon is the basic element of living organisms and is non-toxic, CDs are being investigated widely in pre-clinical studies. Further, for drug delivery applications, nitrogen-doped CDs (N@CDs) are considered as preferred choice. N@CDs are basically nanomaterials with a spherical morphology, characterized by a size of < 10 nm. They offer unique properties such as excellent biocompatibility, low toxicity, tuneable surface functionality, and high surface area, making them attractive drug delivery vehicles. Recent investigations have advocated the use of N@CDs across a range of therapeutic disorders, including cancer, neurological conditions, ocular diseases, infections, gene delivery, etc.[6] The fabrication of N@CDs can be achieved by a one-step facile hydrothermal synthesis technique. Further, the surface of N@CDs is enriched with different functional groups, *viz.* –OH, –COOH, and –NH_2, which facilitates their chemical linkage with various ligands/therapeutic agents/organic molecules, making them highly adaptable for diverse pharmaceutical and biomedical applications.[7,8] Due to the electron-rich nitrogen sites and reactive surface radicals, N@CDs exhibit strong interac-

tions with bacterial cells, making them attractive as antimicrobial agents. In addition, their high therapeutic efficacy, combined with low toxicity, supports their potential use in combating resistant pathogens. Obtaining CDs with different properties depends not only on the synthesis method, but also on the precursors.[9] Both natural and artificial precursors are used in the synthesis of N@CDs, which include small molecules like citric acid, ascorbic acid, glucose, urea, etc., and even waste products.

N@CDs in view of their anti-microbial effectiveness, are being explored for effective management of various bacterial infections.[10] In a study, Zheng and team reported that carbon quantum dots with nitrogen doping (N@CQDs) produced hydrothermally showed moderate inhibition of Gram-positive bacteria in the dark and complete bacterial killing under white light, demonstrating a light-enhanced antimicrobial effect.[11] In another work, N@CDs demonstrated direct antimicrobial action against both *E. coli* and *S. aureus* with measurable minimum inhibitory concentrations (MICs) *in vitro.*[12] In addition, it is reported that N@CDs inhibited both Gram-positive and Gram-negative bacteria, remaining non-toxic to mammalian cells and showed good skin permeation, indicating their efficacy for topical *in vivo* applications.[13–15] Furthermore, N@CDs are widely recognized for generation of reactive oxygen species more efficiently, than conventional CDs promoting notable antioxidant activity that contributes to cellular protection and reduction of oxidative stress within the vaginal microenvironment.[16–19]

Overall, these studies confirm that N@CDs exhibit significant anti-microbial activity *in vitro,* often enhanced by light activation, and show promising potential for *in vivo* applications such as topical formulations. Furthermore, for effective vaginal application, N@CDs may be delivered through specific formulations like suppository, gel, cream, etc. In fact, distribution of therapeutic molecules through these formulations ensures a concentrated localized availability at the vaginal area as compared to oral or injectable administration.[20,21] Among the conventional localized formulations, bio-adhesive suppository-based formulation ensures a high concentration of drugs at the lesion site, improves efficacy, reduces off-target distribution and mitigates adverse effects.[22,23] Vaginal bio-adhesive drug delivery systems establish interaction with the mucosal surface through muco-interactive mechanisms, wherein mucin molecules form a coating on the vaginal mucosa, increasing the residence time of the dosage form at the vaginal site.[24]

As discussed above, *E. coli* mediated BV is the commonest form of bacterial infection at vagina. It has been found that the crucial infection mechanism (adhesion and penetration) of *E. coli* across vaginal epithelium is mediated by a specific protein (Fim-H), expressed heavily on Type-1 pili. D-mannose (DM), a common monosaccharide, is involved in the glycosylation of certain proteins and has been demonstrated to bind to Fim-H protein the of *E. coli*.[25] Thus, application of DM would prevent adherence of *E. coli* over the vaginal epithelium through a competitive inhibition. This interaction of DM-Fim-H in inhibiting *E. coli* infection has been validated in *in vivo* animal models too.[26] While DM shares structural similarities with glucose, the body does not metabolise DM, the same way as it does with glucose. DM may not be absorbed well enough when taken orally; on the other hand, it may act effectively when delivered through a suitable topical delivery system. Many works have already documented the potential role of DM in combating BV. Use of DM in the prophylaxis of recurrent urinary tract infections was reported elsewhere.[27] A study by Joshi and co-workers reported a reduction in cellular senescence along with NLRP3/IL-1β-mediated uroepithelial cell shedding by DM in a murine bladder model.[28]

In view of this, the study aims to develop and evaluate N@CDs loaded suppositories containing DM as a strategy to combat *E. coli* mediated BV. As Fim-H is the unique protein expressed on *E. coli* and mediates crucial infection mechanism, it is hypothesized that application of DM in the formulation would competitively inhibit the natural interaction of Fim-H with mannosylated receptors. This competitive interaction would inhibit adhesion and penetration of *E. coli* over vaginal epithelium. Since Fim-H-DM interaction was the prime target, hence *E. coli* has been specifically selected has the model bacteria for the study. Experimental N@CDs were developed using conventional hydrothermal technique and were evaluated in terms of UV-visible spectroscopy, quantum yield, fluorescence intensity, Raman spectroscopy, X-ray diffraction, HR-TEM, FTIR, average particle size, and zeta potential. The experimental N@CDs were incorporated into a suitable suppository following central composite design optimization. *In vitro* antimicrobial effectiveness of N@CDs loaded suppository was carried out against *E. coli* and *S. aureus*. This non-invasive approach thus holds the potential to improve treatment outcome in BV by providing a localized, sustained nano modality.

2. Materials and methods

Citric acid monohydrate, urea and D-mannose were obtained from Sigma-Aldrich, Germany. Carbopol 934P was procured from Hi-media, Mumbai, India. Gelatin and glycerine were obtained from Nice Pvt.Ltd, Goa, India. Propylene glycol was purchased from Hi-Media, Mumbai, India. All remaining chemicals/reagents utilized in this study were of analytical purity grade.

2.1. Fabrication method of N@CDs

N@CDs were synthesized, via a standard hydrothermal route, employing urea and citric acid as the starting precursor materials under controlled thermal conditions.[29] The experimental N@CDs were synthesized under

optimal reaction conditions, established with a molar ratio of 1:5 (urea to citric acid) and subjected to hydrothermal treatment at 190°C, maintained for 6 hours. 2.5 g citric acid and 0.5–0.54 g of urea (equivalent to 0.1–1 wt%) were dissolved in 30 mL of deionized water. The prepared mixture was agitated thoroughly using a magnetic stirrer for 15 minutes at ambient temperature to ensure homogeneity. The mixture was subsequently transferred into a 100 mL stainless steel hydrothermal autoclave lined with Teflon and subjected to immediate hydrothermal treatment at 170–190 °C for 4–6 hrs. The resulting mixture was then cooled down to ambient temperature, centrifuged at 10,000 rpm for 20 minutes to eliminate bulk particles and then passed through a 0.22 µm syringe membrane and dialyzed using a 20 mL dialysis kit (1kDa molecular weight cut off) against 1.5 L of deionized water, repeated eight times for 48 hours. A resulting pale-yellow solution of N@CDs was obtained and stored at 4 °C for further analytical applications.

2.1.1. *In vitro* characterization of N@CDs

The prepared N@CDs were subjected to comprehensive *in vitro* characterization in order to evaluate their functional efficacy at the laboratory scale. These assessments aimed to establish their therapeutic potency, thereby determining their suitability for subsequent translational investigations, including *in vivo* applications.

2.1.2. UV and fluorescence spectrophotometry

N@CDs were subjected to spectroscopic assessment for the determination of their UV absorbance and fluorescence intensity). UV-visible spectra were obtained by using a Lab India UV-Vis spectrophotometer 3200 (Maharashtra, India). In addition, the fluorescence (FL) measurement was carried out in a standard quartz cuvette with multiple excitation wavelengths (350–500 nm) using a F-4600 fluorescence spectrophotometer (Hitachi, Japan).[30]

2.1.3. Fourier-transform infrared spectroscopy

Spectral characterization via FTIR was employed to characterize the surface chemistry of experimental N@CDs, enabling the identification of distinct functional moieties contributing to their solubility, reactivity and to depict possible interaction between the selected drug and the excipients. Samples of pure N@CDs, selected excipients (gelatin, glycerine, D-mannose) and prepared suppository along with blank formulation (without N@CDs) were mounted onto a zinc selenide crystal and compressed against the attenuated total reflectance crystal (ATR crystal) interface using an integrated pressure application device and analyzed by Bruker infrared analyser (Bruker alpha; Ettlingen, Germany).[31] The samples were evaluated in the range of 4000–500 cm^{-1}.

2.1.4. Quantum yield measurement

The quantum yield measurements for the as-synthesized N@CDs were conducted using an FS5 spectrofluorometer (Edinburgh Instruments), and the calculations were performed by the reference method [32], which used quinine sulphate in 0.1 M H_2SO_4 as the reference (QY=0.54). Certain amounts of N@CDs and quinine sulphate were dissolved in deionized water and 0.1M H_2SO_4. The QY was calculated by the equation outlined below:

$$Quantum\ Yield = QY_{Ref} \times \frac{I}{I_{Ref}} \times \frac{A_{Ref}}{A} \times \frac{\eta^2}{\eta_{Ref}^2} \quad (1)$$

where the quantum yield is indicated by "QY", *"I"* denote the measured integral photoluminescence intensity, and "A" indicates the absorbance. Additionally, "η" denotes the refractive index value of the solvent medium, which was 1.33 for both the quinine sulphate solution as well as the N@CDs aqueous dispersion. The subscript *Ref* refers to the corresponding parameter of quinine sulphate.

2.1.5. Surface morphology and dynamic light scattering (DLS) measurements

The morphological and structural analysis of the fabricated N@CDs was determined by employing a high resolution-transmission electron microscope (HR-TEM) with a JEOL (JEM F 2100 with EDS) (Shanghai, China). Few drops of diluted aqueous dispersion of N@CDs were mounted on a gold grid coated with carbon for the determination of surface morphology.[33] The hydrodynamic diameter and particle size distribution of the experimental N@CDs was characterized by using a Zetasizer Nano ZS (Malvern Instruments, U.K.). ImageJ software was utilized to determine the average diameter and standard deviation.

2.1.6. Zeta potential

Zeta (ζ) potential measurement is the key characterization technique used to determine the surface charge, hydrodynamic size and colloidal stability of nanoparticles, which were measured using a Zeta sizer Pro ZS90 (Malvern Panalytical Ltd., Worcestershire, United Kingdom).[34] A diluted suspension of N@CDs was prepared, in the concentration range of 0.1–1 mg/ml, followed by sonication (5–10 min) in order to ensure a uniform dispersion. The prepared suspension was then filled in a disposable folded capillary cell and inserted into the zeta potential analyzer. The measurement temperature was kept at 25 °C, and typically 3–5 runs were conducted per sample to obtain the average.

2.1.7. Powder X-ray diffraction

The crystallinity of prepared N@CDs was analyzed using the powder X-ray diffraction (XRD), using a D8 Advanced X-ray diffractometer (Bruker, Germany) with a Cu

Kα radiation (operated at 40 kV and 40 mA) at a range of 10 °C to 70 °C, with the step speed of 0.03° s^{-1}.[35]

2.1.8. Raman spectroscopy

Furthermore, Raman spectra were carried out by exciting the CDs at a wavelength between (450–532 nm) along with a slit width of 100 μm and the spectrum was recorded by using a (Horiba Scientific Lab RAM HR., USA).[35]

2.1.9. X-ray photoelectron spectroscopy

To depict the elemental composition of the experimental N@CDs, X-ray photoelectron spectroscopy (XPS) was employed as an important tool. Briefly, dried CDs sample was placed inside a physical electronics spectrophotometer (PHI5700).[36] Using a monochromatic radiation (at 300 W, 15 kV) with a multichannel detector, XPS analysis was carried out within a path mode of 29.35 eV. The resulting spectra were further analyzed using the Multipak package v.9.3.

2.1.10 Nuclear magnetic resonance spectroscopy

For nuclear magnetic resonance spectroscopy (NMR), experimental CDs was dispersed in deuterium oxide (D_2O) and was placed inside an NMR tube. The NMR tube was then placed in an ultrasound apparatus (at 80W for 20 min).[37] The ^1H and ^{13}C NMR spectra of experimental CDs were recorded at 400 MHz and 125 MHz respectively (Bruker Advance III) following which respective chemical shift values (***δ***) were recorded.

2.2. Method of formulation of N@CDs loaded suppository

The formulation development of N@CDs loaded suppository**,** the conventional fusion moulding method was employed with few modifications.[38] Briefly, the precisely measured amounts of gelatin and D-mannose were dissolved in double-distilled water in a beaker. Another beaker containing a known amount of glycerine was heated to 120 °C. The gelatin solution was then poured into the beaker holding the glycerine, and the mixture was heated until it became homogenous. The previously prepared N@CDs solution was then added at a required amount to the obtained homogenous mixture. After chilling in an ice bath, the semisolid mass was poured into a suppository mould that had been previously lubricated. The finished suppositories were gathered into large containers wrapped in butter paper and placed in a cool, dry place till further use.

2.2.1. Central composite design optimization for development of experimental suppository

Preliminary trial and error method were done to select formulation parameters of pessary base. The amount of gelatin, carbopol and propylene glycol were designated as the independent variables, and disintegration time, liquefaction time and mucoadhesive strength were taken as the response variables.

The optimization of experimental suppository formulations was done by using Design Expert Software (Version 13). Based on the experimental studies, the amount of gelatin (X_1), carbopol (X_2) and propylene glycol (X_3) were designated as the independent variables, considered at 3 levels each. Disintegration time (Y_1), liquefaction time (Y_2) and mucoadhesive strength (Y_3) were taken as the response variables.

2.3. Characterization of experimental N@CDs loaded suppository

2.3.1. Physical appearance and size measurement

The physical appearance of the experimental N@CDs loaded suppository was examined through visual inspection. The colour, shape, and surface texture were evaluated visually. The size of the prepared suppository was measured by using a Vernier calliper.[39]

2.3.2. Hardness and melting point

The N@CDs loaded suppository was examined for its level of abrasiveness using a hardness tester. The amount of weight that was needed to cause the suppository to break was taken as the hardness parameter.[40] To determine the melting point, the technique of increasing the melting point was used. The experimental suppository was placed in capillary tubes measuring 10 cm in length, which were sealed at one end and filled to an approximate height of about 1 cm.[41] The tubes were then immersed in an electro-thermal thermometer (Seti Cairo, Egypt) with integrated heating element.

2.3.3. Disintegration test

For the disintegration test, the N@CDs loaded suppository was taken inside the USP disintegration apparatus (Disintegration test apparatus Lab India, Mumbai). Double-distilled water was used as the medium to carry out the disintegration test at 37±5 °C.[42]

2.3.4. Liquefaction time

To carry out this experiment, a test tube was loaded with citro-phosphate buffer (pH 4.5) before being immersed in a water bath at 37 °C. N@CDs loaded suppository was inserted into the test tube from one end and pushed to the other. A slender glass rod was positioned on top of the suppository, and the time taken for the glass rod to make its way through the suppository was noted as the liquefaction time.[43]

2.3.5. Evaluation of anti-microbial effectiveness of N@CDs loaded suppository *in vitro*

The antimicrobial potency of experimental N@CDs loaded suppository was measured from the determination of zone of inhibition (ZOI) as depicted elsewhere.[44,45] Briefly, Muller Hinton agar (38 g) was dissolved in 1000 ml of double-distilled water, followed by autoclaving at 121 °C (15 Lbs) for 15 mins. The medium was then cooled and was then poured into sterilised petri plates (20 mL/plate). Pure cultures of *E. coli*/*S. aureus* (1.5×10^8 CFU/ml) were inoculated into nutrient agar plates. Following an incubation period of 37 °C (24 h), empty sterile paper discs (around 6 mm) were placed on the inoculated media by using sterile forceps. Selected suppositories with different concentrations were introduced into the sterile discs with the help of sterile pipettes. VagiBIOM *Lactobacillus pessary* was introduced in another sterile disc as a standard. The blank suppository was used as the control. Following 24 h incubation, the size of the ZOI was measured in millimetres by using a transparent ruler.

2.3.6. Minimum inhibitory concentration and minimum bactericidal concentration test

Selected bacterial strains, specifically, *E. coli* and *S. aureus,* were subjected to the minimum inhibitory concentration (MIC) as well as minimum bactericidal concentration (MBC) assays. The bacterial cultures are grown overnight in Luria Bertani (LB) broth at 37 °C along with continuous agitation at 180 rpm. Subsequently, the samples were diluted to reach a concentration of 1×10^6 CFU/ml. The as-synthesized N@CDs sample was tested in various concentrations obtained through serial twofold dilutions (e.g., 50, 250, 450 µg/mL). The LB medium alone was taken as a blank, while the bacterial suspension without N@CDs in the LB medium was taken as a control. These mixtures were incubated at a temperature of 37 °C for about 20 hrs in the incubator. Post incubation, the extent of bacterial growth was assessed by the measurement of absorbance at 600 nm (OD600) with a BioTek 800 TS microplate reader, providing an estimate of cell density in each sample. After the determination of MIC, correspondingly the MBC assay was carried out by the sub-culture of 100 µL aliquots from wells that showed no visible growth onto fresh LB plated (without N@CDs). The plates were further incubated at 37 °C for 24 hrs. The least concentration of N@CDs, showing no colony formation was recorded as the MBC value. [46]

2.3.7. *Ex vivo* mucoadhesive strength

To determine the mucoadhesive strength of experimental N@CDs loaded suppository, rabbit vaginal mucosa was used. The force of adhesion between the rabbit mucous vaginal membrane and the tested N@CDs loaded suppository was measured using a modified balance instrument to assess the mucoadhesive qualities of the experimental vaginal suppository.[47,49]

The strength of muco-adhesion is established by:

Adhesion Force (N) = Mucoadhesive strength*9.81/1000

Bond strength (N) = Adhesion Force/ Surface area of formulated suppository

2.3.8. DPPH scavenging assay

The DPPH free radicals scavenging test was used to assess antioxidant capability of N@CDs and N@CDs-DMS. In short, 3 mL of 0.1 mM methanolic DPPH solution was used to distribute N@CDs and N@CDs-DMS at different concentrations between 10 and 50 µg/mL. The solution was left to incubate for half an hour at ambient temperature in a dark environment. At 515 nm, the absorbance of the sample was measured in relation to ascorbic acid (as a standard) and methanolic DPPH (as a blank). The IC_{50} value was used to indicate the antioxidant efficiency.[50] The % inhibition was calculated using the following formula:

$$\% \text{ of inhibition} = \frac{(absorbance\ of\ control - absorbance\ of\ the\ sample)}{absorbance\ of\ control} \times 100$$

3. Results

3.1. Formulation development and characterization of prepared N@CDs

The N@CDs were developed using the conventional hydrothermal synthesis method and characterized.

3.1.1. UV and fluorescence spectrophotometry

The UV-visible spectral analysis of N@CDs exhibited typical absorption band at 332 nm, which were attribut-

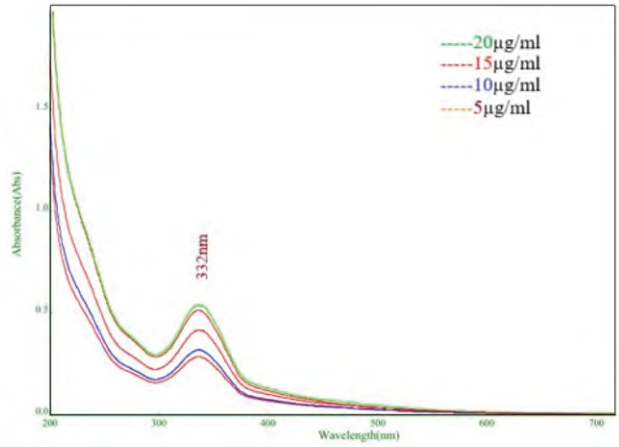


Figure 1: Normalized UV-visible spectrum of experimental N@CDs observed at 332 nm. Different dilutions of N@CDs *viz.* 5 µg/ml, 10 µg/ml, 15 µg/ml, 20 µg/ml

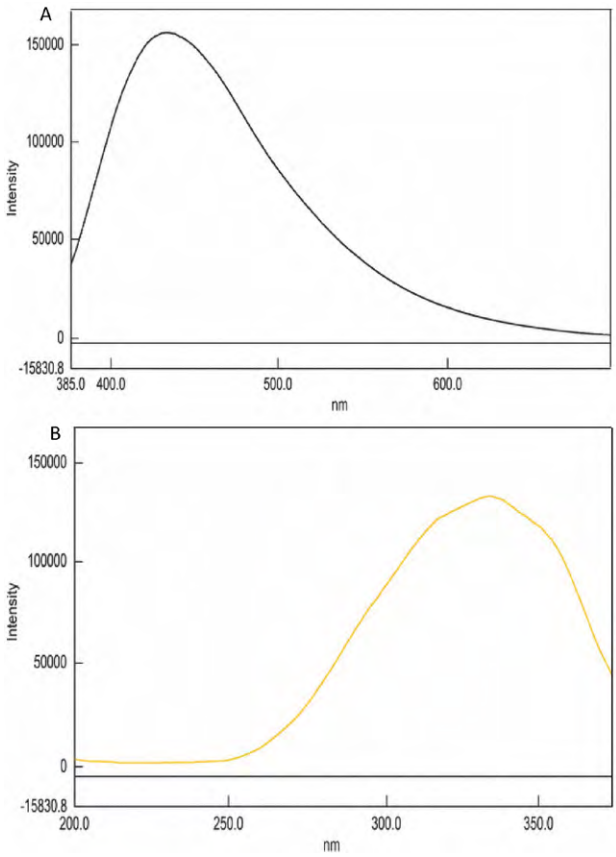


Figure 2: Normalized photoluminescence spectra of prepared N-CDs. A) PL emission spectra. B) PL excitation spectra

ed to the π-π* transitions of the carbon nucleus and the n-π* transitions from C=O bonds with sp^2 hybridization (Fig. 1). The photoluminescence excitation and emission spectra of the fabricated N@CDs are depicted in (Fig. 2). The maximum wavelengths for excitation (λ_{ex}) and emission (λ_{em}) were 334 nm and 434 nm, respectively, which are consistent with the luminescent wavelengths of other CDs published elsewhere. A gradual reduction in emission intensity of N@CDs was observed with an increase in the excitation wavelength, which can be attributed to the diverse distribution of surface states, particle size variations, and the intricate architecture of the experimental N@CDs. Besides, the experimental N@CDs remained visually colourless in solution but emitted bright blue fluorescence upon excitation by sunlight or UV light, highlighting their photoluminescent properties.

3.1.2. Fourier-transform infrared spectroscopy

The FTIR spectrum showed the presence of various surface functional groups of N@CDs. As depicted in (Fig. 3), several absorption peaks were observed in between 4000–500 cm^{-1}. The broad peaks spanning from 3700–2500 cm^{-1} corresponds to N–H and O–H stretching vibrations. The peaks at 1649 cm^{-1}, 1492 cm^{-1},1351 cm^{-1}, 1180 cm^{-1} were ascribed to hydroxyl, C-H bending, C–N stretching, C–O stretching vibrations, respectively. Hence, these findings suggested the presence of hydrophilic $–NH_2$ and –OH functional groups on the surface of N@CDs, contributing to their aqueous dispersibility. Moreover, the $–NH_2$ moiety offers a reactive site for facile conjugation with appropriate ligands. Furthermore, D-mannose showed distinctive peaks at 3304, 3298 and 2916 cm^{-1} linking to O–H stretching, C–H stretching vibration, respectively. For Carbopol, O–H stretching, CH_2 bending and C–OH stretching vibration peaks were observed at 2924, 1451 and 1161 cm^{-1}, respectively. Similarly, gelatin showed its characteristic peaks at 2928 cm^{-1} (C–H stretching) and 1051cm^{-1} (C–O stretching), which signifies the presence of aldehyde and ketonic groups in the structure (Fig. 3). The characteristic peak of the drug (3298 cm^{-1}) was shown to be slightly shifted at 3269 cm^{-1} related to O-–H stretching in the selected suppository formulation. In the formulation, the peaks at 2936 (N–H stretching), 3269 (O–H stretching) and 1642 cm^{-1} (C=C stretching) signified the presence of D-mannose and the selected polymers (gelatin, glycerin). Though there was a minor shifting of characteristic peaks found in the formulation as compared to the individual spectrum, no major interaction was noticed. The minor shifting of peaks in D-mannose and polymer may be attributed to the presence of weak intermolecular forces like van der Waals interactions, hydrogen bonding or electrostatic interactions. However, the absence of any major interaction between the drug and selected excipients justified the physical compatibility for the formulation. The weak interaction forces could be further helpful for successful formulation.

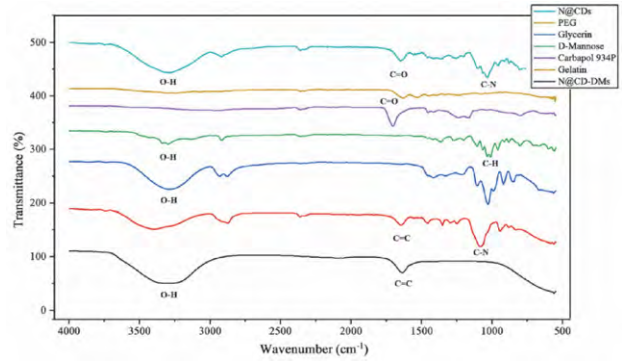


Figure 3: FTIR spectrum of i) N@CDs, ii) PEG, iii) Carbopol 934P, iv) Glycerin, v) D-mannose, vi) Gelatin, vii) N@CD-DMS

3.1.3. Quantum yield measurement

The QY of prepared N@CDs was calculated by comparing integrated photoluminescence intensity at 360 nm, which was kept under slit width 0.05 at excitation wavelength of N@CDs with that of quinine sulphate. Furthermore, the QY was 32.08%, using quinine sulphate as the standard reference compound.

3.1.4. Surface morphology and dynamic light scattering (DLS) measurements

HR-TEM was employed to depict surface morphology, size and texture of the experimental N@CDs. Well formed, spherical, discrete dots were found across the HR-TEM image (Fig. 4a), showing good formulation characteristics. N@CDs were found to have size less than 10 nm (when visualized on a 50 nm scale bar). The average size of N@CDs was further validated and supported from DLS study, where an average diameter of 5.2 nm N@CDs was reported with a distinct uniform distribution. This distinctive structure of N@CDs provides a high surface-to-volume ratio, which is anticipated to enhance their drug loading capacity when used as a nanocarrier. The as-synthesized N@CDs were suspended in ultra-pure water at a concentration of 1 mg/mL, followed by sonication for 10 min, to ensure homogeneous dispersion avoiding aggregation. The DLS analysis showed that the N@CDs had a hydrodynamic diameter of 5.2 ± 0.5 nm with a PDI of 0.18, indicating a narrow size distribution and good monodispersity (Fig. 4b).

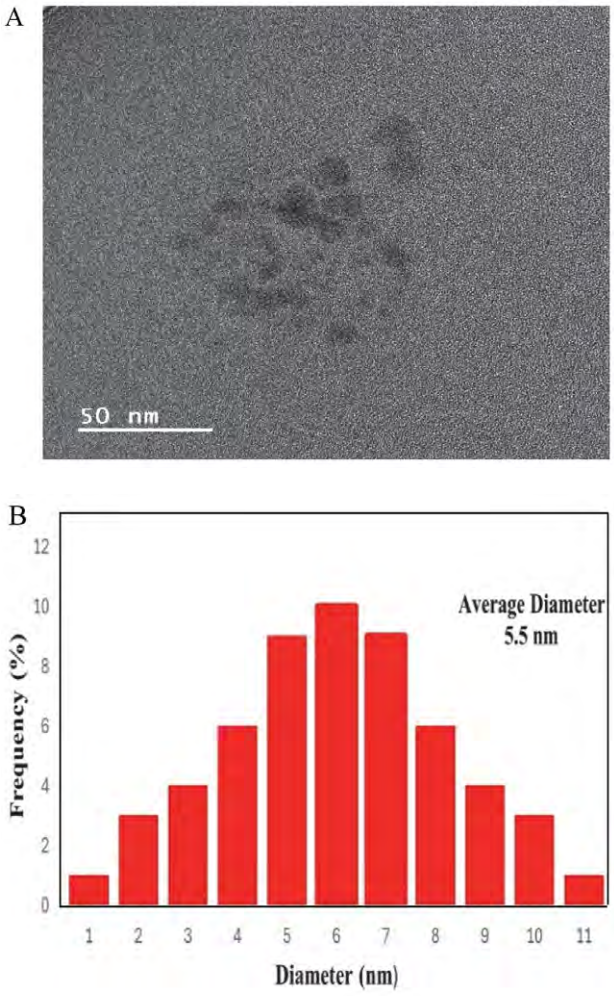


Figure 4: A) HR-TEM images of the N@CDs. B) average particle size of 5 ± 0.5 nm.

3.1.5. Zeta potential

A high ζ potential imparts strong electrostatic repulsion among particles, effectively minimizing the coalescence and contributing to enhanced suspension stability. The ζ potential of the prepared N@CDs was about –16.23 mV, so the N@CDs were stable in solution form (Fig. 5). The (-ve) sign implies the presence of carboxylic and amino groups. Therefore, the enhanced stability of aqueous colloidal system can be attributed to the electrostatic stabilization arising from surface passivation of the synthesized N@CDs passivated by –COOH, OH and $–NH_2$ groups.

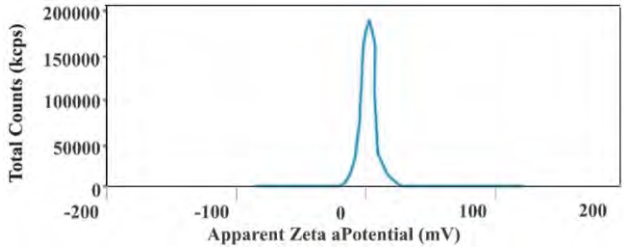


Figure 5: Zeta (ζ) potential distribution data of the prepared N@CDs

3.1.6. X-ray diffraction

For analyzing the XRD pattern of N@CDs, the prepared samples were dried on a glass cover slip, which showed a broad wide diffraction peak at 2θ = 20–23°, which indicates the presence of disordered carbon atoms embedded in an amorphous phase (Fig. 6).

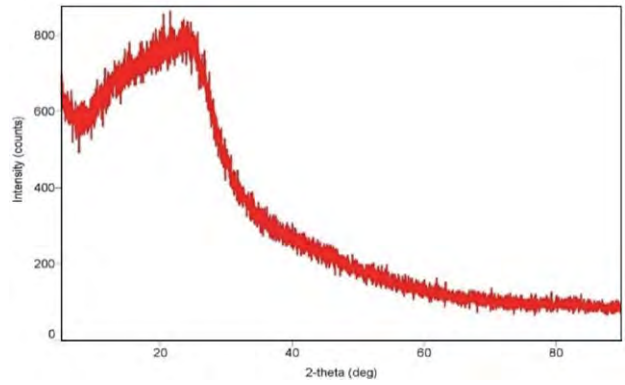


Figure 6: XRD observation of the prepared N@CDs

3.1.7. Raman spectroscopy

The Raman spectra of the synthesized N@CDs revealed two distinct peaks at 1598 and 1345 cm^{-1}, indicating the G and D bands, respectively, validating the existence of carbon-based nanostructures in the form of CDs. The intensity ratio of I_D/I_G was calculated to be 0.84. The D-band is associated with defects and crystalline structural disorder with sp^2 hybridization, whereas the G-band reflects the vibrational mode of graphitic carbon, indicative of well-ordered crystalline regions (Fig. 7).

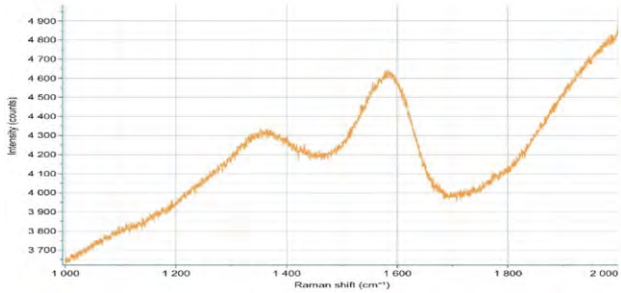


Figure 7: Raman spectrum of prepared N@CDs

3.1.8. X-ray photoelectron spectroscopy

The surface chemical concentration (atom %) of experimental N@CDs revealed three dominant signals corresponding to C1s (~284–285 eV) pertaining to C–C/C=C bonds. Similarly, O1s (~531–533 eV) confirmed the presence of carbonyl and hydroxyl groups and N1s (~399–401 eV) revealed the presence of NH_2 groups, in the experimental CDs (Fig.8). The quantitative analysis also showed carbon as the major constituent (72.6%), followed by oxygen (25.32%) and nitrogen (2.09%).

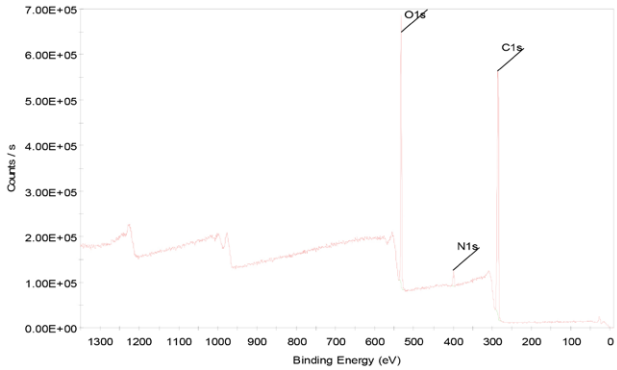


Figure 8: XPS analysis of experimental N@CDs showing elemental composition

3.1.9. Nuclear magnetic resonance spectroscopy

The ^{1}H NMR spectrum of the experimental CDs revealed multiple overlapping resonances between 2.2–3.0 ppm, consistent with methylene groups adjacent to sulfonate and amide functional groups. A distinct signal at ~3.1 ppm was attributed to $–CH_2$ groups bonded to sulfonate moieties. Methyl resonances appeared in the 1.2–1.4 ppm range (Supplementary file 1). The broadness of several peaks indicated aggregation effects and heterogeneous surface environments.

Furthermore, ^{13}C NMR spectrum displayed resonances near 170–173 ppm, characteristic of amide carbonyl carbons. Signals between 60–65 ppm corresponded to methylene carbons adjacent to sulfonate groups, while peaks in the 30–40 ppm range were assigned to aliphatic methylene carbons (Supplementary file 1). The overall spectrum confirmed the presence of amide, carboxylate, and sulfonate functional groups on N@CDs surface, justifying successful formation.

3.1.10 Formulation of experimental suppository by using central composite design optimization

Development of experimental N@CDs loaded suppository was carried out employing central composite de-

Table 1: Actual Design and Runs

Run	Space Type	Factor 1 Gelatin (mg)	Factor 2 Carbopol 934P (mg)	Factor 3 Propylene Glycol (mL)	Response 1 Disintegration Time (min)	Response 2 Liquefaction Time (min)	Response 3 Mucoadhesive Strength (dyne/cm^2 ×10^2)
1	Center	3	1.375	3.5	8.1	10.51	4.9
2	Factorial	4	1	2	10.52	12.04	4.1
3	Axial	3	2.00567	3.5	11.01	12.04	4.1
4	Axial	1.31821	1.375	3.5	11.02	12.05	4.2
5	Center	3	1.375	3.5	8.2	10.53	4.9
6	Factorial	4	1.75	5	10.51	12.03	4
7	Axial	3	1.375	0.977311	11.01	12.04	4.1
8	Axial	3	1.375	6.02269	11	12.03	4
9	Axial	3	0.744328	3.5	8.91	11.66	4.2
10	Center	3	1.375	3.5	8.1	10.51	4.9
11	Factorial	2	1.75	2	10.52	12.01	4.7
12	Center	3	1.375	3.5	8	10.5	4.9
13	Center	3	1.375	3.5	8.1	10.51	4.9
14	Factorial	4	1.75	2	10.5	12.03	4.6
15	Factorial	2	1	2	10.1	11.2	4.5
16	Factorial	2	1.75	5	10.2	11.3	4.6
17	Axial	4.68179	1.375	3.5	10.02	11.75	4.5
18	Center	3	1.375	3.5	8.1	10.51	4.9
19	Factorial	4	1	5	10.1	11.2	4.5
20	Factorial	2	1	5	10.3	11.2	4.5

sign by taking gelatin, carbopol 934 P and propylene glycol as independent variables, whereas disintegration time, liquefaction time and mucoadhesive strength were taken as dependent variables. The concentration of the polymers and plasticizer influence the physicochemical characteristics of the suppository. Thus, carbopol 934 P, gelatin, propylene glycol was selected as the independent variables. Similarly, for effective intravaginal application, mucoadhesive strength, disintegration and liquefaction time are the crucial factors. Hence, those were taken as responses in relation to independent variables. However, the amount of D-mannose and N@CDs remains constant in the suppository formulation, and hence, those were not included as any variables in the optimization process.

Table 2: Independent and dependent variables levels used to fabricate the experimental suppository

Independent variables (Factors)	Levels Low −1	Medium 0	High 1
Gelatin (X_1)	1.32	3.00	4.68
Carbopol (X_2)	0.7443	1.38	2.01
Propylene Glycol (X_3)	0.9773	3.50	6.02
Dependent Variables (Response)			
Disintegration Time (Y_1)	8	9.72	11.02
Liquefaction Time (Y_2)	10.5	11.38	12.05
Mucoadhesive Strength (Y_3)	4	4.50	4.9

3.0.1. Mathematical Modelling for RSM Optimization

The polynomial equation relating the different response and independent variable is given below:

(Y_1) Disintegration Time = $+8.11 - 0.0858X_1 + 0.3106X_2 - 0.0400X_3 + 0.0087X_1X_2 - 0.0363X_1X_3 - 0.0113X_2X_3 + 0.7930\ X_1^2 + 0.5950\ X_2^2 + 0.9645\ X_3^2$

(Y_2) Liquefaction Time $=10.52 + 0.0795X_1 + 0.1735X_2 - 0.1147X_3 - 0.0113X_1X_2 - 0.0163X_1X_3 + 0.0162X_2X_3 + 0.4090\ X_1^2 + 0.3913X_2^2 + 0.4567X_3^2$

(Y_3) Mucoadhesive Strength = $+4.89 - 0.0436X_1 + 0.0097X_2 - 0.0343X_3 - 0.0375X_1X_2 - 0.0125X_1X_3 - 0.1375X_2X_3 - 0.1316X_1^2 - 0.2024\ X_2^2 - 0.2377\ X_3^2$

The above equation represented the quantitative effect of process variables and their interactions on the response. Where, X_1 = conc. of gelatin, X_2 = conc. of carbopol 934 P and X_3 = conc. of propylene glycol.

3.2. 3D response surface plot

To visualize the interaction between independent and dependent variables, 3D response surface plots were constructed using the fitted polynomial model, enabling a detailed assessment of how the response varied across the experimental design space. The effect of X_1, X_2 and X_3 with their interaction on disintegration time, liquefaction time and mucoadhesive strength can be further understood by these plots.

It was observed that a change in the concentration of X_1 led to a change in disintegration time (Fig. 9a). This could be attributed to the higher viscosity of the gelatin during formulations, resulting in changes in disintegration time. However, variation in the concentration of carbopol (X_2) did not bring significant changes in the disintegration time.

Further, it was observed that the liquefaction time decreased with an increase in the concentration of carbopol (Fig. 9b). Also, it was found that the concentration of gelatin (X_1) and Carbopol (X_2) had an antagonistic effect on mucoadhesive strength (Fig. 9c). However, the concentration of carbopol showed a positive impact on mucoadhesive strength.

3.3. Formulation and characterization of N@CDs loaded suppository

Based on the optimization data, suppository was formulated using the predicted amount of carbopol, gelatin and propylene glycol from the central composite design. However, the amount of N@CDs and D-mannose were kept constant. For the formulation, 3 g of gelatin, 1.75 mg of carbopol and propylene glycol were used. Further, to aid liquefaction and elegancy, glycerine (7 mL) was added to the suppository. 200 mg of D-mannose and 0.75 mg of N@CDs were incorporated during formulation.

3.3.1. *In vitro* characterization of experimental N@CDs loaded suppository

3.3.2. Physical appearance and size measurement

N@CDs loaded suppository was found translucent with a smooth texture. There was no roughness on the edges. The suppository was elegant as visually inspected. All the experimental suppository was conical shape with a 4.8–5.0 mm size. Experimental suppository was found homogenous without presence of any agglomeration or insoluble particles on its surface.

3.3.3. Hardness and melting range

To depict the impact of D-mannose on the mechanical strength of the experimental suppository, a hardness test was conducted. The measured hardness of the tested suppository ranged from (141.5±0.1 to 190±0.1 g), indicating optimum mechanical strength suitable for handling, transportation and vaginal insertion (Table 5).

A narrow melting range plays a crucial role in preserving the structural integrity of the suppository at ambient conditions and in regulating the melting time of the suppository after administration. The tested sup-

Table 3: ANOVA summary for effects of formulation variables on specific responses of N@CDs suppositories using central composite design

Response 1: Disintegration time						
Source	**Sum of Squares**	**df**	**Mean Square**	**F-value**	**p-value**	
Model	24.73	9	2.75	15.18	0.0001	**significant**
A-Gelatin	0.1005	1	0.1005	0.5557	0.4732	
B-Carbopol	1.32	1	1.32	7.28	0.0224	
C-Propylene glycol	0.0219	1	0.0219	0.1210	0.7352	
AB	0.0006	1	0.0006	0.0034	0.9548	
AC	0.0021	1	0.0021	0.0174	0.8976	
BC	0.0010	1	0.0010	0.0056	0.9418	
A^2	9.06	1	9.06	50.09	< 0.0001	
B^2	5.10	1	5.10	28.20	0.0003	
C^2	13.41	1	13.41	74.09	< 0.0001	
Residual	1.81	10	0.1809			
Lack of Fit	1.79	5	0.3579	89.47	< 0.0001	**significant**
SPure Error	0.0200	5	0.0040			
Cor Total	26.54	19				
Response 2: Liquefaction time						
Source	**Sum of Squares**	**df**	**Mean Square**	**F-value**	**p-value**	
Model	7.05	9	0.7834	6.46	0.0037	**significant**
A-Gelatin	0.0863	1	0.0863	0.7116	0.4186	
B-Carbopol	0.4110	1	0.4110	3.39	0.0954	
C-Propylene glycol	0.1798	1	0.1798	1.48	0.2513	
AB	0.0010	1	0.0010	0.0084	0.9290	
AC	0.0021	1	0.0021	0.0174	0.8976	
BC	0.0021	1	0.0021	0.0174	0.8976	
A2	2.41	1	2.41	19.88	0.0012	
B2	2.21	1	2.21	18.20	0.0016	
C2	3.01	1	3.01	24.79	0.0006	
Residual	1.21	10	0.1212			
Lack of Fit	1.21	5	0.2424	2507.26	< 0.0001	
Pure Error	0.0005	5	0.0001			
Cor Total	8.26	19				
Response 3: Mucoadhesive strength						
Source	**Sum of Squares**	**df**	**Mean Square**	**F-value**	**p-value**	
Model	1.61	9	0.1789	3.14	0.0445	**significant**
A-Gelatin	0.0260	1	0.0260	0.4558	0.5149	
B-Carbopol	0.0013	1	0.0013	0.0223	0.8842	
C-Propylene glycol	0.0160	1	0.0160	0.2818	0.6071	
AB	0.0112	1	0.0112	0.1975	0.6662	
AC	0.0105	1	0.0105	0.0581	0.8144	
BC	0.1513	1	0.1513	2.66	0.1343	
A2	0.2498	1	0.2498	4.38	0.0627	
B2	0.5901	1	0.5901	10.36	0.0092	
C2	0.8143	1	0.8143	14.30	0.0036	
Residual	0.5696	10	0.0570			
Lack of Fit	0.5696	5	0.1139	12.36	< 0.0001	**significant**
Pure Error	0.0000	5	0.0000			
Cor Total	2.18	19				

Statistical Analysis (Disintegration time)
Experimental data were analyzed using response surface methodology (RSM). The model's significance was confirmed by an F-value of 15.18, indicating a low probability (0.01%) of the result arising from random variation. Model terms B, A^2, B^2, and C^2 were statistically significant (P-values < 0.0500), while terms with p-values above 0.10 were considered non-significant. Lack of Fit F-value of 89.47 further supported the robustness of the model, with minimal likelihood of error due to random variation.

Statistical Analysis (Liquefaction time)
Experimental data were analyzed using response surface methodology (RSM). The model's significance was confirmed by an F-value of 6.46, indicating a low probability (0.37%) of the result arising from random variation. Model terms B, A^2, B^2, and C^2 were statistically significant (P-values < 0.0500), while terms with p-values above 0.10 were considered non-significant. Lack of Fit F-value of 2507.26 further supported the robustness of the model, with minimal likelihood of error due to random variation.

Statistical Analysis (Mucoadhesive strength)
Experimental data were analyzed using response surface methodology (RSM). The model's significance was confirmed by an F-value of 3.4, indicating a low probability (4.45%) of the result arising from random variation. Model terms B, A^2, B^2, and C^2 were statistically significant (P-values < 0.0500), while terms with p-values above 0.10 were considered non-significant. Lack of Fit F-value of 12.36 further supported the robustness of the model, with minimal likelihood of error due to random variation.

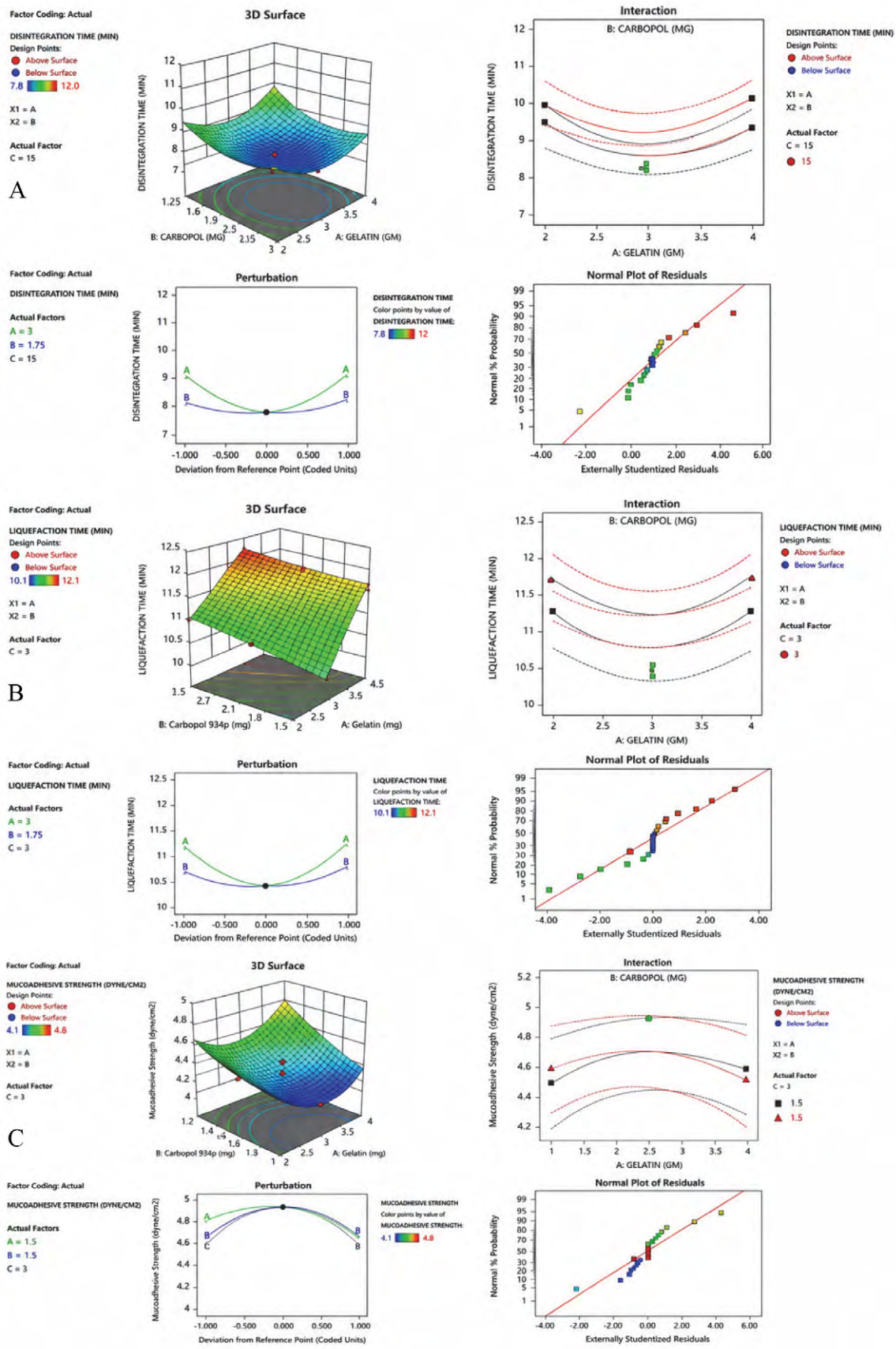


Figure 9: Central composite design depicting the effect of formulation parameters on A) Disintegration time, B) liquefaction time and **C**) Muco-adhesive strength of experimental N@CDs-DM loaded pessaries.

Table 4: Results of central composite design applied on N@CDs loaded suppository

Analysis	Model-derived Mean	Model-derived Median	Observed	Std Dev	n	SE Pred	95% PI low	Data Mean	95% PI high
Disintegration time	8.09489	8.09489	8.10052	0.425372	1	0.459215	7.07169	8.10052	9.11808
Liquefaction time	10.501	10.501	10.51129	0.348185	1	0.375886	9.66342	10.51129	11.3385
Mucoadhesive strength	4.88754	4.88754	4.91451	0.238672	1	0.257661	4.31343	4.91451	5.46164

pository showed a satisfactory melting point at 38.6–39.2 °C.

3.3.4. Disintegration test

The experimental N@CDs loaded suppository showed a reasonable disintegration time of 8.1 min complied with the disintegration time limit as per British Pharmacopoeia. The disintegration time for water-soluble suppositories should not exceed 60 minutes, as declared by the B.P. (2007). Thus, in view of lower disintegration time, the experimental suppository would show timely release of components upon *in vivo* application.

3.3.5. Liquefaction time

The liquefaction test determines the time needed for a pessary to liquefy under pressures similar to those found in the vagina in the presence of dissolution buffer pH 4.5 at 37±0.5 °C. A suppository penetration test was used to measure the temperature at which the suppository becomes sufficiently soft for a penetrating rod to bore across its length. The data showed liquefaction times for the tested suppositories were within the desired range (Table 5).

Table 5: Evaluation of physicochemical characteristics of experimental N@CDs loaded suppositories

N@CDs suppo sitory	Hardness (gm)	Liquefaction time (min)	Mucoadhesive strength (dyne/cm^2 × 10^2)	Disintegration time (min)	Melting range (°C)
	182±0.22	10.51	4.9±0.20	8.10	38.6–39.2

Data expressed as Mean ± SD

3.3.6. Anti-microbial effectiveness of N@CDs loaded suppository *in vitro*

Antimicrobial effectiveness of the experimental N@CDs/ N@CDs loaded suppository was investigated from the measurement of ZOI. In the disc diffusion method, the absence of ZOI was considered as the absence of antimicrobial activity. Usually, the activities were expressed as resistant if the ZOI was less than 7 mm, intermediate (if ZOI in between 8–10 mm) and sensitive (if ZOI ≥ 11 mm).[46] Data showed an effective inhibition zone for both the tested bacteria, *E. coli* and *S. aureus*. (Fig. 10) We have selected *S. aureus* along with the target bacteria (*E. coli*) to predict a comparative efficacy study of the experimental N@CDs. In both cases, reasonable inhibition of bacterial growth was visible, and the effect was even comparable to the standard drug therapy. The study overall confirmed the effective antibacterial potential of the experimental formulation in combating *E. coli* and *S. aureus* growth *in vitro*.

3.3.7. Minimum inhibitory concentration and minimum bactericidal concentration test

The MIC and MBC values for the selected species of bacteria following exposure with N@CDs/N@CDs-DM are depicted in Fig. 10 and Table 6. Experimental CDs depicted efficient antimicrobial activity against both the tested bacteria. Further, the anti-microbial activity results were corroborated by the comparable diameters of the ZOI observed for both *E. coli* and *S. aureus*. The MIC data confirmed that the N@CDs effectively suppressed the growth of the selected bacteria, at a minimum concentration of 50 μg/mL and 75 μg/mL for N@CDs. Presence of DM further contributed towards the antimicrobial potency of N@CDs. The MBC data also showed similar trend at the concentration of 150 μg/mL, substantial healing of *E. coli* was observed. For *S. aureus*, 156 μg/mL was reported as the effective MBC value. Further it was noticed that incorporation of DM resulted further suppression of bacterial growth as shown in Table 6. Overall, it was confirmed that inclusion of DM brought a decline in bacterial cell viability. The preferential antimicrobial activity towards both the tested bacteria could be attributed to the generation of reactive oxygen species (ROS).

3.3.8. *Ex vivo* mucoadhesive strength

The bio adhesive force is an important parameter for experimental N@CDs loaded suppository since it affects the gelled solutions from reaching the end of the vaginal cavity. If the adhesive force is too excessive, the supposito-

Table 6: Measurement of minimum inhibitory concentration (MIC) and minimum bactericidal concentration (MBC) of experimental N@CDs against *S. aureus* and *E. coli*.

Bacteria	MIC (µg/mL) N@CDs loaded suppository	MIC (µg/mL) N@CDs-DM loaded suppository	MBC (µg/mL) N@CDs loaded suppository	MBC (µg/mL) N@CDs-DM loaded suppository
E. coli	50	35	150	131
S. aureus	75	57	156	148

Data expressed as mean± SD

ry can damage the vaginal epithelial membrane. Therefore, these suppositories must possess an optimum bio-adhesion. N@CDs loaded suppository showed the highest bio-adhesion, i.e. (4.9×10^2 dyne/cm^2). (Table 5)

2.3.9. DPPH scavenging assay

Ability of N@CDs and N@CDs-DMS to scavenge free radicals on DPPH was computed as a percentage of inhibition, as shown in Fig. 11. N@CDs and N@CDs-DMS showed a scavenging effect similar to that of standard ascorbic acid. Compared to N@CDs, the N@CDs-DMS had a much greater antioxidant impact. At 50 µg/mL, the ascorbic acid, N@CDs and N@CDs-DMS inhibition percentages were 97.36±1.77%, 74.83±2.3 %, and 86.66±1.23%, respectively. The corresponding IC_{50} values of ascorbic acid/N@CDs and NCDs-DMS were found as 16.33±2.3, 30.79±1.5, and 21.71±1.7 µg/mL, respectively.

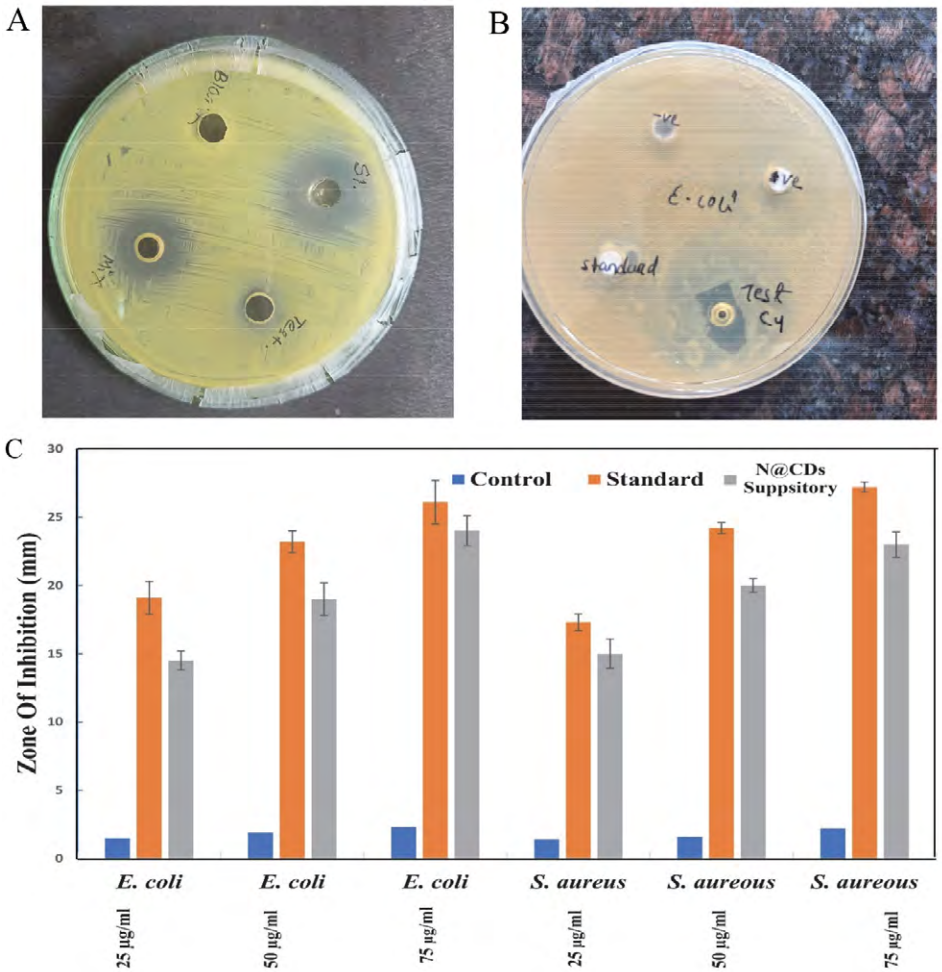


Figure 10: Evaluation of *in vitro* antimicrobial effectiveness of selected experimental N@CDs loaded suppository against *E. coli* (B) and *S. aureus* (A) from the measurement of the zone of inhibition. A blank suppository was taken as a control. (C) Data are represented as mean ± SD (n = 3). *p < 0.05 compared with differentiated control.

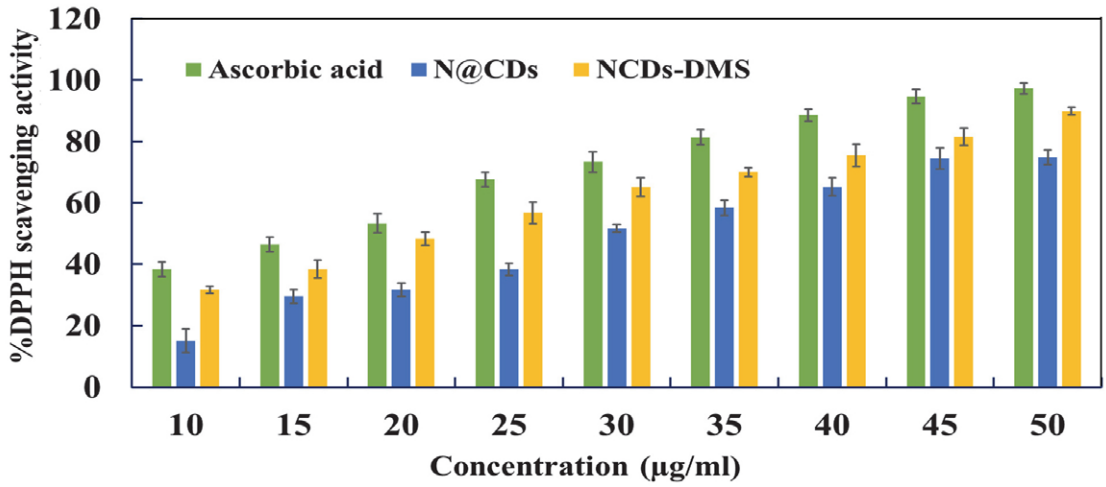


Figure 11: DPPH radical scavenging activity

The study overall indicated a higher antioxidant potential of N@CDs-DMS as compared to N@CDs.

4. Discussion

N@CDs have garnered significant attention owing to their promising applications as anticancer agents and as dual-modality platforms for imaging and photothermal therapy. Moreover, the integration of these compounds into pharmaceutical formulations, particularly hydrogels, has demonstrated promising outcomes in antibacterial and wound healing applications.[51] Despite these advancements, there is still a significant lack of evidence regarding their therapeutic efficacy in the context of vaginal infections. There is a notable gap in understanding the interactions between N@CDs and pathogens in simulated vaginal microenvironments, especially when these interactions are analyzed in relation to glycerol-gelatin suppositories that include DM for Fim-H targeting. In light of this notable research gap, our investigation focuses on the development of DM incorporated suppository containing experimental N@CDs. Application of DM would supress the adhesion of *E. coli* over the vaginal epithelium through interaction with Fim-H protein. Additionally, the N@CDs would exert their antibacterial effect. Thus, the work aims to deliver critical insights on application of CDs and DM in novel topical formulation for vaginal infection.

The study reported a facile hydrothermal synthetic method for the production of N@CDs, where citric acid was used as a source of carbon, and urea as an agent of surface passivation. The conventional hydrothermal synthesis method was proved effective for producing stable as well as biocompatible N@CDs. Nitrogen-doped CDs are being heavily investigated owing to their exceptional fluorescence properties. The presence of nitrogen over the surface of CDs confers a negative charge due to the deprotonation of surface carboxyl and hydroxyl groups. When these surface modalities are introduced into an acidic environment, they get protonated, increasing the positive charge, which efficiently interacts with the hydrophobic domains on the negatively charged bacterial membranes and kills the bacterial population through the generation of reactive oxygen. In the study, the N@CDs were successfully synthesized, which was confirmed by UV-Vis spectroscopy from the appearance of absorption bands at 239 nm and 332 nm. The absorption bands depicted π-π^* transitions of the carbon nucleus and the n-π^* transitions from C=O bonds with sp^2 hybridization, which is one of the characteristic features of N@CDs. Further confirmation of the formation of N@CD was established by photoluminescent spectral analysis, where high fluorescence intensity of 434 nm ($\boldsymbol{\lambda}_{em}$) was observed against 334 nm ($\boldsymbol{\lambda}_{ex}$).

FTIR analysis was conducted to depict the presence of important functional groups in N@CDs. Presence of –OH, $–NH_2$, and –COOH groups were detected from FTIR spectrum, which further confirmed the successful formation of the carbon dot structure. The quantum yield, an essential feature of fluorescent nano structures, was found to be 32.08% (at 360 nm) for experimental N@CDs in comparison that of quinine sulphate. Higher value of quantum yield thus signified the integrated photoluminescent property of N@CDs. The satisfied photoluminescent property of experimental N@CDs would be helpful for their *in vivo* imaging/diagnostic applications. The average size of N@CDs was around 5.2 nm, as depicted from Dynamic light scattering measurement. The ultra-nano size of experimental N@CDs would be helpful to penetrate efficiently across bacterial cell wall or to rupture bacterial biofilm. Further a higher negative surface charge (–16.23 mV) of N@CDs indicates good colloidal stability due to electrostatic repulsion. The amorphous nature of the N@CDs was validated by the XRD patterns as broadened, blunt were observed for experimental N@CDs. Absence of sharp peaks in the XRD spectrum indicates amorphization of N@CDs. The amorphous nature promotes higher solubility of N@CDs. Raman spectroscopy has now been accepted as an inhabitable tool for structural characterization of N@CDs. The ob-

tained Raman spectrum depicted presence of D and G bands, which are typical characteristic features of Sp^2 and Sp^3 hybridized carbon core. Thus, Raman spectroscopy overall confirmed partial graphitization.

XPS further elucidated elemental composition of experimental N@CDs. Appearance of C1s, O1s and N1s signals referred to the presence of hydroxyl/carbonyl/amine groups, which overall confirmed successful formation of N@CDs with active surface functional groups. Further, the elemental composition highlighted the desired nitrogen doping, which could be linked to the superior antimicrobial potency observed *in vitro.* These findings further validated potential interaction of experimental N@CDs with the bacterial membrane.

The NMR spectra further rationalized XPS analysis report. The ^{1}H NMR and ^{13}C NMR signals confirmed the presence of amide, carboxylate, and sulfonate functional groups, which could be contributing factor to attain colloidal stability and to provide reactive sites for bacterial biofilm disruption. The broadness of several peaks indicated heterogeneous surface environments, consistent with the multifunctional potential of N@CDs. Together, these data strengthen the mechanistic rationale that N@CDs can act as both antimicrobial agents and nanocarriers owing to the presence of surface-active functional groups. The as-synthesized N@CDs were incorporated into experimental suppository formulation following process optimization. Central composite design predicted the optimized parameters of disintegration time, liquefaction time and mucoadhesive strength, keeping gelatin and carbopol 934 P as the independent variables. The model was found to be significant which helped to appropriately design the experimental suppository formulation. From the above ANOVA tables, it was derived that all the models are significant. The p-value less than 0.0500 indicates model terms are significant. Lack of fit was also significant. Gelatin concentration negatively influenced the disintegration time of the suppositories. This could be attributed to the higher viscosity of the gelatin during formulations, leading to changes in disintegration time. However, variation in the concentration of carbopol made significant changes in disintegration time. A reduction in liquefaction time was observed, with an increase in the concentration of carbopol 934 P. Additionally, factor X_3 negatively affected the liquefaction time. The concentration of gelatin and propylene glycol inversely affected the mucoadhesive strength. However, the concentration of carbopol 934 P showed a positive impact on mucoadhesive strength.

The FTIR analysis confirmed the absence of any sort of strong chemical interactions between N@CDs and excipients used in the suppository, supporting compatibility of N@CDs with selected excipients. The minor peak shifts observed were likely due to weak hydrogen bonding or van der Waals forces, which may aid in controlled drug release. The optimized N@CDs loaded suppository demonstrated ideal physical and functional characteristics, including rapid liquefaction (10.51 min) under simulated conditions, acceptable disintegration time (8.10 min), and strong mucoadhesion (4.9 dyne/cm^2). Furthermore, the DPPH activity of N@CDs-DMS depicted strong antioxidant potential as compared to N@CDs. DPPH is a stable free radical that can scavenge a free electron or hydrogen atom to form a more stable diamagnetic molecule. The antioxidant activity of N@CDs and N@CDs-DMS in scavenging DPPH free radicals was evident from the observed colour change of DPPH solution from purple to pale yellow. Lower IC_{50} value of N@CDs and N@CDs-DMS depicted potential free radical scavenging activity. The scavenging effects of N@CDs-DMS were higher than N@CDs, which further confirmed the radical scavenging potency.

These properties are critical for ensuring localized retention and effective delivery of N@CDs in the vaginal microenvironment. Thus, the optimized N@CDs suppository in view of satisfied physicochemical characteristics would enhance therapeutic action of N@CDs.

The antimicrobial studies (*in vitro*) revealed that N@CDs possess broad-spectrum activity against both Gram-negative (*E. coli*) and Gram-positive (*S. aureus*) bacteria. The potential of N@CDs to inhibit microbial growth may be attributed to successful disruption of bacterial membranes via reactive oxygen species and electrostatic interactions, consistent with previous reports on carbon-based nanomaterials. Functional groups existing on the N@CDs surface are believed to interfere with key enzymatic pathways within the bacterial cells, thereby suppressing their proliferation and contributing to the observed antimicrobial effect. The presence of delocalized π- conjugated domains/electron systems in N@CDs promotes efficient electron exchange with bacterial surfaces, enhancing their ability to adhere onto the cell walls and exert antimicrobial effects.[52] Furthermore, the superior MBC efficacy highlights the synergistic action of N@CDs-DM, ensuring complete microbial eradication.

Chandrasekaran, R *et al.* in a recent study reported wound healing potential of carbon dots.[53] Another study reported potent bio-imaging and antifungal effect of green synthesized carbon dots.[54] CDs loaded gel were also designed and investigated for anti-cancer application against breast and skin melanoma cell lines.[55,56] However, no such reports on carbon dots specifically towards *E. coli*-mediated vaginal infection is there. The integration of D-mannose would enhance the formulation's specificity/efficacy towards *E. coli* through the Fim-H adhesin protein. In addition, mucoadhesive nature of optimized suppository would ensure prolonged retention of N@CDs across the vaginal epithelium to elicit the desired localized action.

5. Conclusion

The present study demonstrates N-doped carbon dots-loaded mucoadhesive suppository as an alternative

and unique approach to address *E. coli*-mediated vaginosis. The successful synthesis of N@CDs through facile hydrothermal method was reported. The as-synthesized N@CDs were ultra nano sized with positive surface charge and photoluminescent property. The XRD study demonstrated the amorphous nature of N@CDs. Further, the presence of D and G bands in Raman spectrum indicated graphitization. Selection of optimized suppository through central composite design showed desirable weight, homogeneity, hardness, melting point, disintegration time, liquefaction time. Satisfactory results of bio-adhesion and liquefaction would be beneficial for effective vaginal application of N@CDs loaded experimental suppository. The effective antimicrobial action of N@CDs against *E. coli* advocates the possibility for potential *in vivo* application in vaginosis. However, toxicity and *in vivo* efficacy analysis of experimental N@CDs suppository in an animal model are highly warranted.

Declaration

The authors of the manuscript have no conflict of interest to declare.

Funding Declaration

No grant from public agencies, or commercial entities was awarded for this research.

Ethics Declaration

Not applicable. This study did not involve animal subjects, human participants or any data seeking ethical approval.

Acknowledgement

The authors are highly thankful to the institute for providing necessary support and encouragement.

Data availability statement

All the data presented in the manuscript can be made available on request and there is no third party associated with the data.

Further, the authors declare no conflict of interest or financial interest whatsoever associated with any third party or organization with the data.

All the data presented in the manuscript can be freely made available at Corresponding author's ORCID 0000-0002-3532-721X

6. References

1. K. Peebles, J. Velloza, J. E. Balkus, R. S. McClelland, R. V. Barnabas, *Sex. Transm. Dis.* **2019**, *46*, 304–311. **DOI:**10.1097/OLQ.0000000000000982
2. Banerjee R, Singh BS, Sahrawat N, Mehrotra A, Swain S, Mishra RM, Antony P, Aparna U, Jain BK, Neogi SB, *BMC Pregnancy Childbirth*. **2025**, *25,* 294. **DOI:**10.1186/s12884-025-07416-3
3. C. A. Muzny, P. Kardas, *Sex. Transm. Dis*. **2020**, *47,* 441–446. **DOI:**10.1097/OLQ.0000000000001178
4. R. Khedkar, S. Pajai, *Cureus*. **2022**, *14*–e0000. **DOI:**10.7759/cureus.31314
5. M. Fang, L. Lin, M. Zheng, W. Liu, R. Lin, *J. Mater. Chem. B*. **2023**, *11*, 9386–9403. **DOI:**10.1039/D3TB01543B
6. P. Lagonegro, C. Marzuoli, G. Tullii, F. Rossi, C. Bellacanzone, E. Mancinelli, *J. Mater. Chem. B.* **2025**, *13*, 2029–2041. **DOI:**10.1039/D5TB90104A
7. Q. Zhang, S. Xie, Y. Yang, Y. Wu, X. Wang, J. Wu, *J. Anal. Methods Chem*. **2018**, 7890937. **DOI:**10.1155/2018/7890937
8. S. Lu, S. Guo, P. Xu, X. Li, Y. Zhao, W. Gu, *Int. J. Nanomed*. **2016**, *11*, 6325–6336. **DOI:**10.2147/IJN.S119252
9. S. Strickland, L. Fourroux, D. Pappas, *Adv. Ther*. **2024**, *8*, 2400366. **DOI:**10.1002/adtp.202400366
10. F. Lin, Z. Wang, F. G. Wu, *Pharmaceuticals* **2022**, *15*, 1236. **DOI:**10.3390/ph15101236
11. W. Xia, Z. Wu, B. Hou, Z. Cheng, D. Bi, L. Chen, *Mater. Today Bio*. **2025**, *30*, 101428. **DOI:**10.1016/j.mtbio.2024.101428
12. J. Liang, W. Li, J. Chen, X. Huang, Y. Liu, X. Zhang, *ACS Appl. Bio Mater*. **2021**, *4*, 6937–6945. **DOI:**10.1021/acsabm.1c00655
13. J. Shangguan, Z. Wu, C. Qiao, Y. Zhang, L. Li, Q. Li, *ACS Omega* **2024**, *9*, 7034–7042. **DOI:**10.1021/acsomega.4c06869
14. A. Saravanan, M. Maruthapandi, P. Das, S. Ganguly, S. Margel, J. H. Luong, *ACS Appl. Bio Mater*. **2020**, *3*, 8023–8031. **DOI:**10.1021/acsabm.0c01104
15. V. B. Kumar, M. Lahav, E. Gazit, *J. Mater. Chem. B*. **2024**, *12*, 2855–2868. **DOI:**10.1039/D3TB02488A
16. Wang S, Chu K, Zhou X, *J. Mol. Struct*. **2026,** *1352*, 144504. **DOI:**10.1016/j.molstruc.2025.144504
17. Gao F, Liu J, Gong P, Yang Y, Jiang Y, *Chem. Eng. J*. **2023,** *462*, 142338. **DOI:**10.1016/j.cej.2023.142338
18. Wu Z, Xia W, Ou L, Zheng L, Hou B, Pan T, Sun W, Koole LH, Shao Y, Qi L, *Int. J. Nanomed.* **2024**, *19*, 2691–2708. **DOI:**10.2147/IJN.S445398
19. Zhang X, Xin Y, Wang H, Dang Y, Wang W, Gao Y, Han Y, Kang R, Shi Q, Du H, *Int. J. Mol. Sci.* **2025**, *26*, 9916. **DOI:**10.3390/ijms26209916
20. B. Ballou, S. K. Andreko, E. Osuna. Highley, M. Mc. Raven, T. Catalone, M. P Bruchez, *PLoS One*. **2012**, *7*, e51995. **DOI:**10.1371/journal.pone.0051995
21. S. K. Tammina, L. Jyothi, J. V. Kumar, H. Srivastava, S. R. Naraharisetty, *Diamond Relat. Mater*. **2024**, *144*, 111013. **DOI:**10.1016/j.diamond.2024.111013
22. N. Upret, R. B. Thapa, *World J. Pharm. Pharm. Sci*. **2024**, *13*, 468–478. **DOI:**10.20959/wjpps20248-27954
23. E. O. Shatabayeva, D. B. Kaldybekov, Z. A. Kenessova, R. N. Tuleyeva, S. E. Kudaibergenov, V. V. Khutoryanskiy, *AAPS PharmSciTech*. **2025**, *26,* 63. **DOI:**10.1208/s12249-025-03055-1

24. B. Valamla, P. Thakor, R. Phuse, M. Dalvi, P. Kharat, A. Kumar, *J. Drug Delivery. Sci. Technol*. **2022**, *70*, 103162. **DOI:**10.1016/j.jddst.2022.103162
25. O. A. Gromova, I. Y. Torshin, N. K. Tetruashvili, *J. Obstet. Gynecol.Reprod*. **2019**, *13*, 119–131. **DOI:**10.17749/2313-7347.2019.13.2.119-131
26. G. Riemma, D. Vinci, M. La. Verde, F. M. Caniglia, G. Scalzone, M. Torella, *Expert Rev. Anti-Infect. Ther*. **2025**, *23*, 523-530. **DOI:**10.1080/14787210.2025.2487162
27. E. Corrales. Acosta, E. Cuartiella. Zaragoza, M. Monzó. Pérez, S. Benítez. Perdomo, J. G. Corrales. Riveros, M. Corrales, *Microbiol. Res*. **2025**, *16*, 66. **DOI:**10.3390/microbiolres16030066
28. C. S. Joshi, A. M. Salazar, C. Wang, M. M. Ligon, R. R. Chappidi, B. E. Fashemi, *Dev. Cell*. **2024**, *59*, 33–47. **DOI:**10.1016/j.devcel.2024.01.002
29. S. Zhu, Q. Meng, L. Wang, J. Zhang, Y. Song, H. Jin, *Angew. Chem.* **2013**, *52*, 3953–3957. **DOI:**10.1002/anie.201300519
30. Y. Q. Liu, L. Liang, C. Huang, Y. Wang, M. Han, Q. F. Hu, *Spectrochim. Acta, Part A*. **2025**, *332*, 125816. **DOI:**10.1016/j.saa.2025.125816
31. Zaca. Moran. O., Díaz. Monge. F, Rodríguez. Juárez. A, Gómez. Muñoz.C. L, Zaca. Moran. P, Secundino. Sánchez O, Díaz. Reyes. J, *Results Chem*. **2024**, *11*, 101788. **DOI:**10.1016/j.rechem.2024.101788
32. A. Tadesse, M. Hagos, D. Rama Devi, K. Basavaiah, N. Belachew, *ACS Omega*. **2020**, *5*, 3889–3898. **DOI:**10.1021/acsomega.9b03175
33. D. M Sam, M. Vergheese, *Indian J. Biochem. Biophys*. **2021**, *58*, 590–601. **DOI:**10.56042/ijbb.v58i6.57791
34. L. Wang, H. S. Zhou, *Anal. Chem*. **2014**, *86*, 8902–8905. **DOI:**10.1021/ac502646x
35. H. Qi, L. Qiu, X. Zhang, T. Yi, J. Jing, R. Sami, *RSC Adv*. **2023**, *13*, 2663–2671. **DOI:**10.1039/D2RA07150A
36. R. Atchudan, T. N. Edison, Y. R. Lee, *J. Colloid Interface Sci.* **2016,** *482*, 8–18. **DOI:**10.1016/j.jcis.2016.07.058
37. G. Gentile, M. Mamone, C. Rosso, F. Amato, C. Lanfrit, G. Filippini, M. Prato, *ChemSusChem.* **2023**, *16*, e202202399. **DOI:**10.1002/cssc.202202399
38. H. Hathaway, S. Milo, J. M. Sutton, T. A. Jenkins*, Ther. Delivery* **2017**, *8*, 543–556. **DOI:**10.4155/tde-2017-0040
39. A. Bassi, G. Sharma, P. K. Deol, R. S. Madempudi, I.P. Kaur, *Gels*. **2023**, *9*, 244. **DOI:**10.3390/gels9030244
40. M. Ghazwani, U. Hani, R. A. Osmani, M. Rahamathulla, M. Y. Begum, S. Wahab, *Int. J. Polym. Sci*. **2021**, *2021*, 9198387. **DOI:**10.1155/2021/9198387
41. P. Rahmanian. Devin, M. R. Fadaei, M. Mashreghi, V. R. Askari, *Saudi Pharm. J*. **2023**, *31*, 101849. **DOI:**10.1016/j.jsps.2023.101849
42. M. M. Pashayan, H. G. Hovhannisyan, *Drug Dev. Ind. Pharm.* **2021**, *47*, 1424–1431. **DOI:**10.1080/03639045.2021.2001485
43. A. D. Mustapha, F. M. Oyedepo, O. D. Akin Ajani, O. A. Odeku, *Futur J. Pharm. Sci*. **2023**, *9*, 80. **DOI:**10.1186/s43094-023-00533-w
44. O. N. Volkova, E. V. Amel'chenko, O. V. Makeeva, S. A. Tolmachev, E. A. Lesovaya, L. C. Zacharia, A. V. Dikovskiy, *BMC Women's Health* **2025**, *25*, 77. **DOI:**10.1186/s12905-025-03616-3
45. V. Vivekanandan, Z. H. Khan, G. Venugopal, B. Musunuru, P. Mishra, S. Srivastava, *Sci. Rep*. **2024**, *14*, 3317. **DOI:**10.1038/s41598-024-53770-1
46. B. S. Satapathy, A. Mishra, S. K. Biswal, S. Pattnaik, R. Parida, B. Biswal, T. K. Shaw, *J. Microencapsulation* **2024,** *41,* 327–344. **DOI:**10.1080/02652048.2024.2354234
47. S. Salatin, M. Tarzamani, A. Farjami, M. Jelvehgari, *Ther Delivery* **2022**, *13*, 95–108. **DOI:**10.4155/tde-2021-0069
48. B. Mohite, R. Patel, N. Kayande, R. Thenge, *J. Pharm. Res. Int*. **2021**, *33*, 123–133. **DOI:**10.9734/jpri/2021/v33i51A33476
49. B. S Satapathy, B. Biswal, S. Pattnaik, R. Parida, R. N. Sahoo. *Int. J. Pharm*. **2023**, *648*, 123542. **DOI:**10.1016/j.ijpharm.2023.123542
50. K. Rajendiran, Z. Zhao, D. S. Pei, A. Fu, *Polymers* **2019**, *11*, 1670. **DOI:**10.3390/polym11101670
51. L. Wang, M. Li, W. Li, Y. Han, Y. Liu, Z. Li, *ACS Sustain. Chem. Eng*. **2018**, *6*, 12668–12674. **DOI:**10.1021/acssuschemeng.8b01625
52. L. Li, Y. Wang, S. Hu, X. Chang, Q. Ding, K. Wang, Y. Chen, J. Zheng, *Acta Biomater*. **2025**, *195*, 467–478. **DOI:**10.1016/j.actbio.2025.01.045
53. R. Chandrasekaran, U. Ushani, G. Sankar, J. Joseph, K. Natarajan, S. Palani, P. Sridhar, R. Nagaraj, S. Sagadevan, *J. Bionanosci.* **2025**, *15*, 1–21. **DOI:**10.1007/s12668-024-01717-1
54. A. Mishra, B. S. Satapathy, P. K. Sahu, *Discover Nano*. **2026,** *21*, 89. **DOI:**10.1186/s11671-026-04528-3
55. M. A. Sheikh, R. S. Chandok, K. Abida, *Discover Nano*. **2023**, *18*, 132. **DOI:**10.1186/s11671-023-03910-9
56. C. L. Savin, C. Tiron, E. Carasevici, C. S. Stan, S. A. Ibanescu, B. C. Simionescu, C. A. Peptu, *Pharmaceutics* **2019**, *11*, 303. **DOI:**10.3390/pharmaceutics11070303

Povzetek

Učinkovito zdravljenje bakterijske vaginoze (BV) ostaja še danes velik izziv. Ta študija predlaga novo strategijo, ki temelji na z dušikom dopiranih ogljikovih pikah (N@CDs), vgrajenih v vaginalni supozitorij z D-manozo. N@CDs so bile sintetizirane z enostopenjsko hidrotermalno metodo in okarakterizirane z uporabo HR-TEM, določanja velikosti delcev (5,2 nm), zeta potenciala (–16,23 mV), rentgenske praškovne difrakcije (XRD), fotoluminiscenčne intenzitete in Ramanske spektroskopije. Supozitorij, optimiziran z metodo centralnega kompozitnega načrta, je bil ovrednoten glede trdote, tališča (35–40 °C), razpadanja, mukoadhezije (4,9 ± 0,20 dyne/ $cm^2 \times 10^2$) utekočinjenja (10,5 min) ter primerne protibakterijske aktivnosti. Analiza FTIR je potrdila odsotnost večjih interakcij med pomožnimi snovmi. Nadaljnje *in vivo* študije na živalskem modelu BV trenutno potekajo za oceno prihodnje klinične uporabnosti eksperimentalnih N@CDs.

Except when otherwise noted, articles in this journal are published under the terms and conditions of the Creative Commons Attribution 4.0 International License